Analysis of laser-induced breakdown spectroscopy spectra: The case for extreme value statistics ☆

Anna P.M. Michel*, Alan D. Chave

*Department of Applied Ocean Physics and Engineering, Woods Hole Oceanographic Institution, Mail Stop 7,
266 Woods Hole Road, Woods Hole, MA, 02543, United States*

Abstract

In most instances, laser-induced breakdown spectroscopy (LIBS) spectra are obtained through analog accumulation of multiple shots in the spectrometer CCD. The average acquired in the CCD at a given wavelength is assumed to be a good representation of the population mean, which in turn is implicitly regarded to be the best estimator for the central value of the distribution of the spectrum at the same wavelength. Multiple analog accumulated spectra are taken and then in turn averaged wavelength-by-wavelength to represent the final spectrum. In this paper, the statistics of single-shot and analog accumulated LIBS spectra of both solids and liquids were examined to evaluate whether the spectrum averaging approach is statistically defensible. At a given wavelength, LIBS spectra are typically drawn from a Frechet extreme value distribution, and hence the mean of an ensemble of LIBS spectra is not necessarily an optimal summary statistic. Under circumstances that are broadly general, the sample mean for LIBS data is statistically inconsistent and the central limit theorem does not apply. This result appears to be due to very high shot-to-shot plasma variability in which a very small number of spectra are high in intensity while the majority are very weak, yielding the extreme value form of the distribution. The extreme value behavior persists when individual shots are analog accumulated. An optimal estimator in a well-defined sense for the spectral average at a given wavelength follows from the maximum likelihood method for the extreme value distribution. Example spectra taken with both an Echelle and a Czerny–Turner spectrometer are processed with this scheme to create smooth, high signal-to-noise summary spectra. Plasma imaging was used in an attempt to visually understand the observed variability and to validate the use of extreme value statistics. The data processing approach presented in this paper is statistically reliable and should be used for accurate comparisons of LIBS spectra instead of arithmetic averaging on either complete or censored data sets.
© 2007 Elsevier B.V. All rights reserved.

Keywords: Laser-induced breakdown spectroscopy; LIBS; Generalized extreme value distribution

1. Introduction

Laser-induced breakdown spectroscopy (LIBS) is a spectro-chemical technique that has been successfully used for elemental analysis of solids, liquids, gases, and aerosols, and is finding increasing application in basic and applied research. However, one of the major problems that precludes more quantitative use is a lack of reproducibility of spectra at a given wavelength on a shot-to-shot basis.

Dramatic peak intensity fluctuations at the shot-to-shot level, suggesting the presence of high random variability, has been noted by many LIBS researchers [1–15]. There are numerous potential causes for this, including repetitive laser pulse instability, unstable laser pulse characteristics, laser pulse-plasma interactions, lens-to-sample distance variation (which in turn changes the distance from the plasma to the collection fiber), laser–material coupling, variable sample ablation, plasma position instability, matrix effects, perturbations of the plasma due to physical and chemical characteristics of the sample (i.e., composition, homogeneity, roughness, color, and moisture

content), scattering of light, atmospheric conditions, weak ionization of the plasma, and non-optimal collection of plasma emission [1,3–11,16]. Optical instability affects the ablation process, the plasma profile, and the plasma volume [7]. Carranza and Hahn [16] suggest that above a threshold value, absorption of pulse energy by the plasma saturates, reducing variability at higher levels. A given plasma is not completely homogeneous, and there may be property gradients due to boundary effects and its transient nature. Spatial variation in the position of the plasma changes the coupling of the plasma light into the collection optics. Carranza and Hahn further suggest that shot-to-shot variation may be reduced by using sufficient laser pulse energy to achieve saturation and a suitable collection geometry (backscatter mode) to minimize spatial variability. The intensity of the laser itself can fluctuate by 1–5% [8]. However, Castle et al. simultaneously measured the analyte signal and the laser pulse energy, and found no significant correlation, suggesting laser pulse variance has only a minor influence on overall variability [13].

The sample type also influences variability. For aqueous samples, additional fluctuation can be caused by "moving breakdown" that changes the distance between the spark and the collection fiber as the plasma moves in the solution. The plasma typically expands along the beam path toward the laser, inducing elongate plasmas that cavitate radially [17]. Variability in aqueous solutions can also be caused by suspended ablated particles [2,18] and bubbles [19] both by reducing the energy delivered to a sample and the light transmitted to the collection optics. Bubbles, formed when breakdown occurs, and dissolved gases can scatter or absorb incident laser radiation [17,19].

Lazic et al. [2] report high variability of the plasma intensity for both aqueous solutions (including bulk water) and solid samples immersed in water. Significant variability was not observed when high laser pulse energies were used to measure the elemental composition of flat homogeneous solid samples. In aqueous solution, LIBS emission was sometimes not detectable even when the maximum laser energy was used. The lack

of emission was also observed for rough inhomogeneous solids. For flat samples, the only time no breakdown occurred was when low laser energies were used; yet, shot-to-shot signal variability was always present. Lazic et al. [10] reported peak intensity histograms. The distributions of these data sets are clearly not Gaussian, and show that a very high intensity peak is a rare event, with very low intensity occurring for the bulk of the trials.

For a solid sample, inhomogeneity, porosity, or surface roughness can change the distance between the focusing optics and the sample, either from prior crater formation or by changing the location of ablation. Panne et al. [12] report significant pulse-to-pulse variation of the plasma electronic excitation temperature and electron density from material–laser interaction for homogeneous glass samples.

Laser ablation is highly nonlinear, and even more so in aerosol samples as the plasma may form at different positions along the beam [8]. For aerosols, the location of the particles within the plasma volume and the focal volume of the optics contribute to variability [14]. Schechter's [15] analysis of spectral fluctuations of aerosols showed large shot-to-shot variability possibly caused by laser pulses hitting different numbers of particles, particle characteristic variation (size, mass, and location), and location variation of the plasma.

Whatever the cause of observed LIBS intensity variability, analog averaging of multiple plasma emissions, where light from numerous laser shots is accumulated on a CCD to create a single spectrum, is an often used experimental approach in order to increase the signal and the signal-to-noise ratio in the presence of shot-to-shot variability [20]. Analog averaged spectra are replicated and the ensemble of replicates are in turn averaged to create a representative spectrum. However, this implicitly assumes that the sample mean is a reasonable estimator for the statistical average, and this condition may not hold for some non-Gaussian distributions.

LIBS researchers have recognized the potential impact of intensity variability, and have devised a variety of methods to reduce the effect of spectral variability. Schechter used a
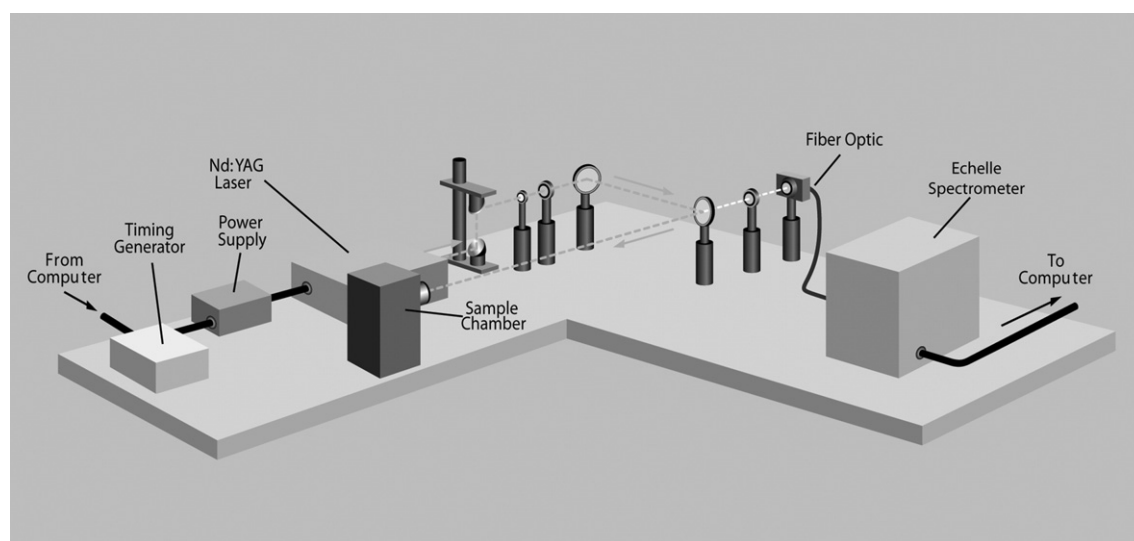

Fig. 1. Laboratory set-up of LIBS using an Echelle spectrometer.

rejection algorithm to eliminate anomalous spectra (e.g., spectra with no elemental lines, spectra with a too weak or too intense baseline due to laser fluctuations, and weak spectra) from the ensemble. This typically removed 75% of measured spectra [15]. Carranza and Hahn [16] used a sorting algorithm to remove irregular spectra, eliminating 60–70% of single shot data. Lazic et al. [2] removed spectra below a threshold value to increase the signal-to-noise ratio and make emission lines more readily visible.

In the present work, rather than using an ad hoc approach, the statistical variability of LIBS spectral intensity has been quantified and a data processing scheme based on the observed statistics has been devised. It will be demonstrated that LIBS intensity (whether single shot or analog averaged) typically has a Frechet extreme value distribution, and that for the characteristic range of statistical parameters, the distribution may not possess a variance. As a consequence, the sample mean is not an appropriate estimator for the average intensity, the central limit theorem does not apply, and Gaussian-based inference will be in error. Instead, a maximum likelihood estimator for the extreme value distribution is advocated as an alternative. The result is illustrated using single shot and analog averaged LIBS spectra for a solid target using one experimental set-up and for bulk aqueous solutions using two experimental set-ups.

2. Experimental

2.1. Echelle spectrometer set-up

To examine the variability of LIBS at shot-to-shot and analog averaged levels, the peak intensity was examined over the 580–600 nm range for Na using both solid NaCl (halite) obtained from Fisher Scientific and an aqueous NaCl solution. Solutions were made using de-ionized water and NaCl to yield a Na concentration of 100 parts per million (ppm, wt./vol.). The variability of intensity was measured for the solid sample using an Echelle spectrometer and for aqueous solutions using both Echelle and Czerny–Turner units. A dark background spectrum was initially subtracted from all raw spectra. For the halite specimen, 100 single shot and 10 shot analog averaged spectra were obtained. For the aqueous specimen, 100 single shot and 100 shot analog averaged spectra were collected.

The first experimental set-up utilizing an Echelle spectrometer (LLA Echelle ESA 3000) is shown in Fig. 1. The spectrometer is capable of detecting elements over the 200–780 nm range with a spectral resolution of 10 to 50 pm. A Big Sky CFR-200 Nd:YAG laser (7.5-ns pulse duration) operated at the fundamental wavelength of 1064 nm with a repetition rate of 5 Hz was used for plasma excitation. The laser is equipped with a variable attenuator controlled by a computer that allows laser pulse energy to range from 0 to 200 mJ in increments of <1 mJ. A timing box (Berkeley Nucleonics Corporation Model 565) was used to accurately control firing of the laser in relation to turn-on of the spectrometer.

For liquid samples, a cubic titanium sample chamber (8.89 cm×8.89 cm×8.89 cm) equipped with two sapphire windows (Meller Optics — 2.54 cm diameter×0.64 cm thick, AR coated at 1064 nm, custom part) that allows laser pulses to enter the cell and the plasma to be imaged from the side of the cell (orthogonal to the entering laser beam) was used. AR-coated optics focus the laser beam into the chamber. For solid samples, the chamber was removed and the final focusing lens was placed in front of the sample. Additional optics were used to focus the plasma light onto an optical fiber that delivers it to the spectrometer. Data were collected using ESAWIN software. All spectra were taken with a pulse energy of 80 mJ and the maximum MCP amplification of 4000. For aqueous NaCl solutions, the delay time=75 ns and integration time gate=200 ns. For halite samples, the delay time=10,000 ns and integration time gate=100 ns.

Plasma images were taken using a Pixelfly camera with a microscope lens and an iris diaphragm. The images were taken through the sapphire window on the pressure chamber, orthogonal to the incoming laser pulses (80 mJ/pulse). The shutter remained open for 5 μs and was externally synched to the Q-switch of the laser.

2.2. Czerny–Turner spectrometer set-up

The second set-up used a Czerny–Turner spectrometer and is shown in Fig. 2. A Continuum Surelite III laser (5-ns pulse duration, 1064 nm, 1 Hz repetition rate) was used for plasma excitation with a pulse energy of 81 mJ. Laser pulses were focused into a chamber constructed of stainless steel Swagelok fittings with six 2.54 cm-ID and 3.18 cm-OD ports. Two ports were fitted with 2.54 cm diameter, 0.32 cm thick circular sapphire windows (MSW100/125, Meller Optics Incorporated) held in place by hex nuts and sealed with rubber washers, allowing 1.91 cm of each window to be visible outside the cell. The plasma emission was focused onto a 2-mm-core-diameter, 0.51-N.A. light guide (Edmund Scientific Co. Model 02551). The light guide was connected to a 0.25-m, f/4 spectrograph (Chromex model 250is/RF) with a 1200-groove/mm grating blazed at 500 nm. Data were collected on an intensified CCD detector (Princeton Instruments, I-Max 1024E) and acquired with a computer running WinSpec/32 software.

All spectra were taken at the maximum gain setting of 255, with delay time=175 ns and integration time gate=200 ns.
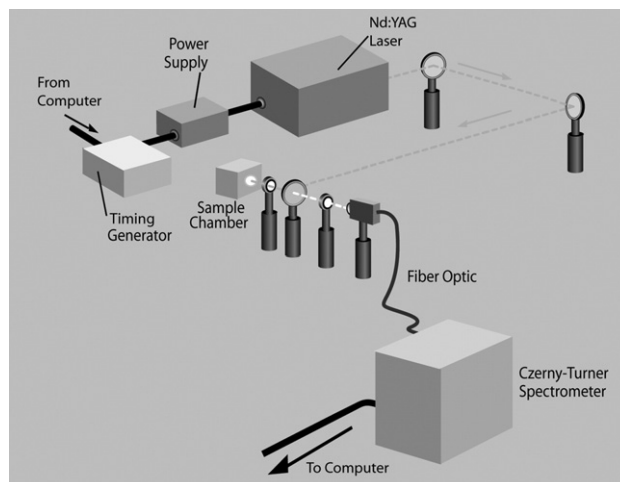

Fig. 2. Laboratory set-up of LIBS using a Czerny–Turner spectrometer.

Solutions were made using de-ionized water, $MnSO_4$, $ZnBr_2$, and $NaSO_4$. The solution contained 5000 parts per million (ppm, wt./vol.) Mn, 5000 ppm Zn, and 2000 ppm Na.

3. Results and discussion

3.1. The generalized extreme value distribution

Extreme value distributions describe the stochastic behavior of the maximum or minimum of independent and identically distributed random variables drawn from some parent distribution. There are three types of extreme value distributions: Weibull, Gumbel, and Frechet. The von Mises–Jenkinson or generalized extreme value distribution (GEVD) combines the three into a single functional form [21,22]. The probability density function for the GEVD is given by

$$f(x|k, \mu, \sigma) = \left(\frac{1}{\sigma}\right) \exp\left(-\left(1 + k\frac{(x - \mu)}{\sigma}\right)^{-\frac{1}{k}}\right)$$
$$\left(1 + k\frac{(x - \mu)}{\sigma}\right)^{\left(-1 - \frac{1}{k}\right)} \quad (1)$$

where the distribution is Weibull, Gumbel and Frechet for the shape parameter $k<0$, $k=0$, and $k>0$, respectively. The remaining parameters in Eq. (1) are the location parameter μ (analogous to the mean for the Gaussian distribution) and the scale parameter σ (analogous to the standard deviation for the Gaussian distribution). The Gumbel distribution is obtained through an appropriate limiting process, but is not of interest in the present work. For the Weibull and Frechet distributions, the range of the variate is respectively $-\infty < x \leq \mu - \sigma/k$ and $\mu - \sigma/k \leq x < \infty$. The Weibull distribution has a finite upper endpoint and hence corresponds to a short-tailed parent. The Frechet distribution has a polynomially decreasing upper tail and corresponds to a long-tailed parent.

As will subsequently be shown, LIBS intensities are typically distributed as Frechet extreme value. It is important to note that the second and higher order moments (and hence the variance) do not exist for $k>1/2$, and the first moment (the mean) does not exist for $k>1$. This implies that the standard estimator for the ensemble average, the sample mean, will either be inconsistent (i.e., will not display a reduced variance as the size of the sample increases) for $k>1/2$ or will not exist at all for $k>1$. A different formulation is required to obtain the three parameters in Eq. (1) so that defensible statistical inferences about LIBS intensities can be made. A standard approach is the maximum likelihood method that seeks the solutions for k, μ and σ that maximize the joint distribution of a given set of data, or the likelihood function. For independent samples, the joint distribution of N data is the product of Eq. (1) for each datum with common shape, location and scale parameters

$$L(k, \mu, \sigma|x_i) = \prod_{i=1}^{N} \left(\frac{1}{\sigma}\right) \exp\left(-\left(1 + k\frac{x_i - \mu}{\sigma}\right)^{-\frac{1}{k}}\right)$$
$$\left(1 + k\frac{x_i - \mu}{\sigma}\right)^{-1-\frac{1}{k}} \quad (2)$$

This is maximized by setting the first derivative of Eq. (2), or its logarithm, for each parameter to zero, yielding a set of three equations

$$\frac{1}{\sigma} \sum_{i=1}^{N} \left[-\left(1 + \frac{k(x_i - \mu)}{\sigma}\right)^{-\left(\frac{1}{k}+1\right)} + \frac{k+1}{1 + k\frac{(x_i-\mu)}{\sigma}}\right] = 0 \quad (3)$$

$$\frac{1}{k^2}\left[\sum_{i=1}^{N} \log\left(1 + k\frac{x_i - \mu}{\sigma}\right) - k\left((1+k)\sum_{i=1}^{N} \frac{x_i - \mu}{\sigma\left(1 + \frac{k(x_i-\mu)}{\sigma}\right)}\right)\right.$$
$$\left. + k\sum_{i=1}^{N} \left(1 + \frac{k(x_i - \mu)}{\sigma}\right)^{-\frac{1}{k}}\left(\frac{\log\left(1 + \frac{k(x_i-\mu)}{\sigma}\right)}{k^2} - \frac{(x_i - \mu)}{k\sigma\left(1 + \frac{k(x_i-\mu)}{\sigma}\right)}\right)\right] = 0$$
$$(4)$$

$$-\frac{N}{\sigma} + \sum_{i=1}^{N} \left[-\left(\frac{\mu - x}{\sigma^2}\right)\left(1 + k\left(\frac{x_i - \mu}{\sigma}\right)\right)^{-\left(\frac{1}{k}+1\right)}\right. \quad (5)$$
$$\left. - \left(1 + \frac{1}{k}\right)\left(\frac{1}{1 + k\left(\frac{x_i-\mu}{\sigma}\right)}\right)\left(\frac{k}{\sigma^2}\right)(\mu - x_i)\right] = 0$$

These are coupled and nonlinear, and must be solved iteratively for the maximum likelihood estimators (mles) $\hat{k}$, $\hat{\mu}$ and $\hat{\sigma}$ using an appropriate algorithm. For the GEVD, the mles are asymptotically efficient (loosely speaking, highly concentrated about the true value for large numbers of data), normal and unbiased, but are neither unbiased nor fully efficient for finite samples. However, neither is the sample mean when the second and higher moments do not exist. The mles have the distinct advantage of being defined when the moments of the distribution do not exist, and are relatively easy to compute. Presuming that the extreme value distribution is a good fit to LIBS intensity data, the maximum likelihood estimate for the location parameter $\hat{\mu}$ is a good representation of the peak intensity at a given wavelength, and the scale parameter $\hat{\sigma}$ and asymptotic normality can be used to compute approximate confidence intervals on $\hat{\mu}$.

3.2. Applicability of extreme value statistics

Quantile–quantile (q–q) plots will be used to demonstrate that LIBS intensities are typically distributed as the Frechet extreme value distribution. The N quantiles of a target distribution are the abscissa values that divide the area under the pdf into $N+1$ equal probability intervals. They are easily obtained from the pdf by solving for Q_j in

$$\int_{-\infty}^{Q_j} f(x)dx = \frac{j - \frac{1}{2}}{N} \quad (6)$$

where $j=1,..., N$. The order statistics of the intensity data are obtained by sorting them into ascending order. The order statistics divide the area under the target pdf into intervals that will correspond to equal probability if the data are drawn from it, and hence a plot of the quantiles against the order statistics will be a straight line. Systematic departures of the data from the distribution are visible as changes in slope, and anomalous
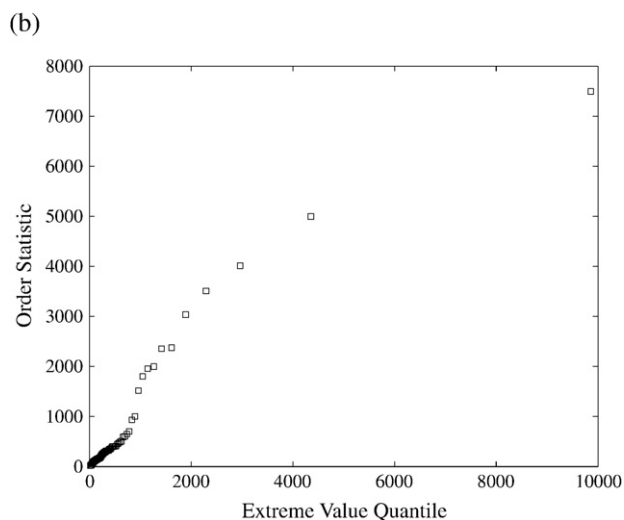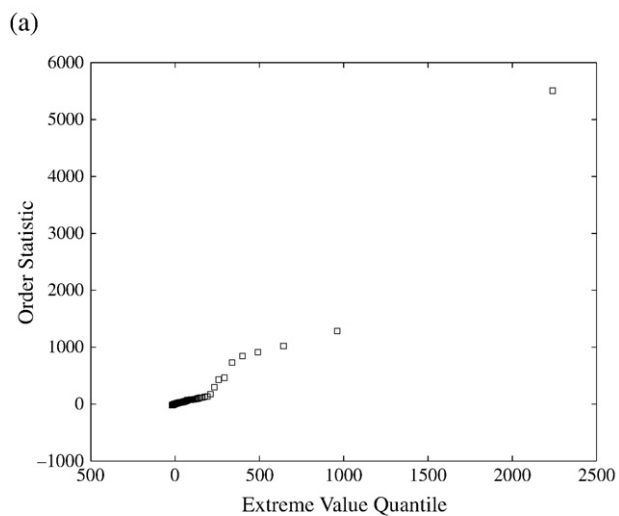
(a)

(b)

Fig. 3. q–q plots for the 588.9953 nm Na I peak for halite using the Echelle set-up. (a) Single Shot (b) 10 Shot Accumulations.

values or outliers are manifest at the extremes, and hence a q–q plot is a useful qualitative tool to assess the suitability of the target distribution as a statistical model.

The fit may be quantified by testing the null hypothesis that the data are drawn from the target distribution against the alternate hypothesis that they are not using the nonparametric Kolmogorov–Smirnov statistic [23] that compares the empirical and target cumulative distribution functions. The Kolmogorov–Smirnov test statistic may be assessed at the standard 0.95 level for which the critical value is 0.134 for 100 realizations, as were used throughout this work. The null hypothesis is rejected if the test statistic exceeds the critical value.

Fig. 3 shows q–q plots for the 588.9953 nm Na I peak for single shot and 10 shot analog accumulations on halite using the Echelle set-up. Both are approximately straight, and both accept the null hypothesis that the extreme value distribution is correct (Kolmogorov–Smirnov test statistics of 0.067 and 0.066, respectively). Fig. 4 shows q–q plots at the same wavelength for single shot and 100 shot analog accumulations for Na in bulk aqueous solution using the Echelle set-up. The single shot data

exhibit a shift in slope that reflects the fact that the vast majority of the data correspond to no signal, and hence are only instrument noise. The 100 shot analog accumulations are slightly short-tailed at the upper end. Nevertheless, both pass the Kolmogorov–Smirnov test with test statistics of 0.113 and 0.098, respectively. Fig. 5 compares q–q plots at the same peak for single shot and 100 shot analog accumulations using the Czerny–Turner set up with a bulk aqueous target. Both are slightly short-tailed at the top of the distribution, but both accept the null hypothesis that the data are extreme value (Kolmogorov–Smirnov test statistics of 0.084 and 0.058, respectively). Similar results are observed for the 589.5923 nm Na peak (not shown), or at other wavelengths where signal is present. Further, the shape parameter persistently lies in the region corresponding to the Frechet extreme value distribution, and in many instances exceeds 0.5 so that the variance does not exist.

3.3. Extreme value statistical parameters

As a demonstration of the importance of using an appropriate set of statistical estimators for LIBS intensity data, the extreme
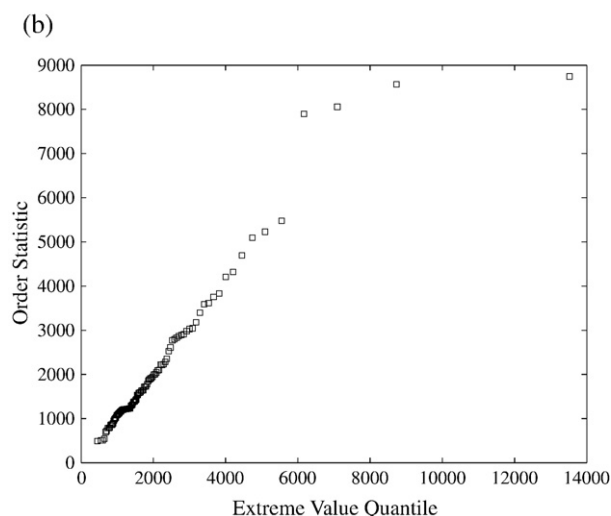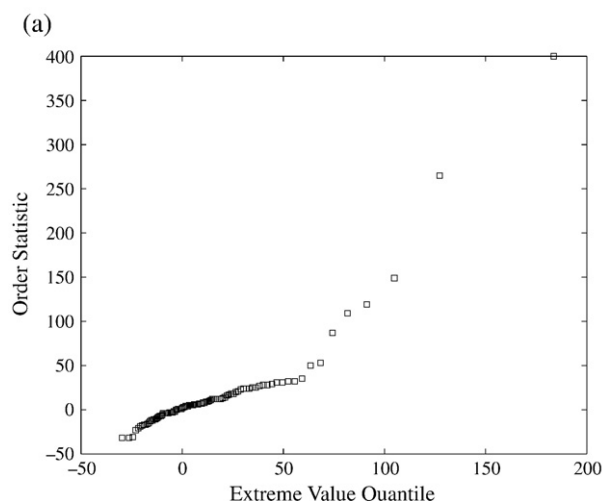
(a)

(b)

Fig. 4. q–q plots for the 588.9953 nm Na I peak for bulk aqueous solution using the Echelle set-up. (a) Single Shot (b) 100 Shot Accumulations.
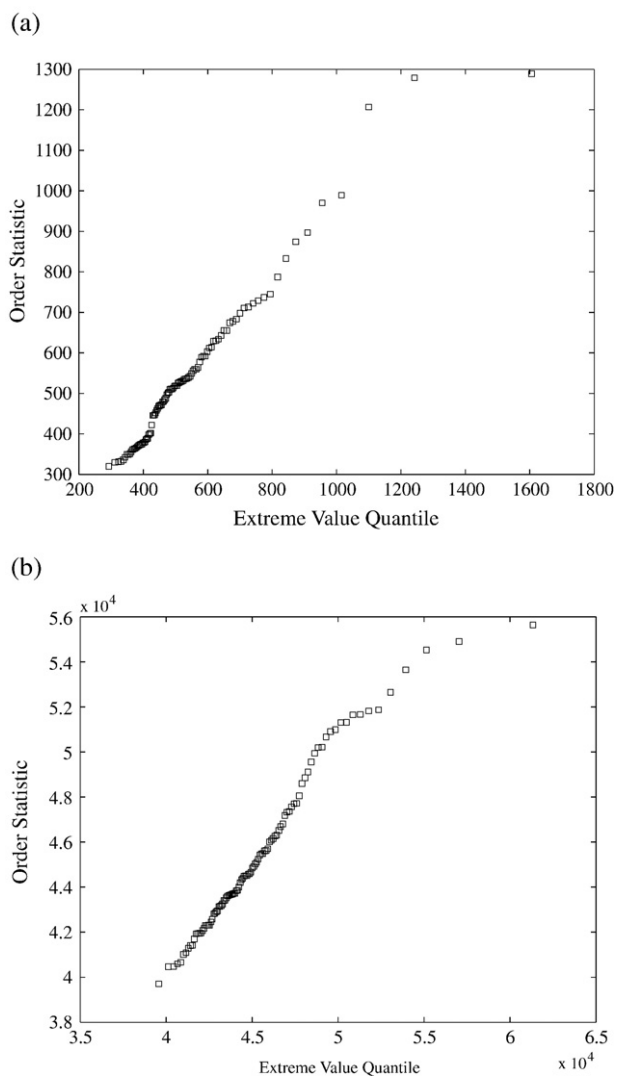
(a)

(b)

Fig. 5. q–q plots for the 588.9953 nm Na I peak for bulk aqueous solution using the Czerny–Turner set-up. (a) Single Shot (b) 100 Shot Accumulations.

value mles and the sample mean were computed over the wavelength band 578.5–605.9 nm for the halite and aqueous Na samples using both the Echelle and Czerny–Turner set-ups. At each wavelength, 100 realizations of 10 (halite) or 100 (aqueous samples) analog-accumulated shots serve as the data from which the mles (Eqs. (3)–(5)) and the sample mean are estimated.

Fig. 6 compares the shape parameter, the location parameter, and the sample mean for halite using the Echelle set-up. While there is wavelength-by-wavelength statistical variability, the shape parameter is persistently above the 0.5 threshold beyond which the variance does not exist, and frequently exceeds the 1.0 threshold beyond which the mean does not exist, especially in the vicinity of the 589 nm Na doublet and over two bands slightly above 600 nm. The extreme value location parameter produces a smooth representation of the LIBS spectrum with limited statistical variability that is consistent with the number of samples. By contrast, the sample mean displays substantial statistical variability with two anomalous nulls amid the Na doublet band. These correspond to the wavelengths where the

shape parameter dips below 1.0, so that the mean becomes defined. For data that are long-tailed, such as those drawn from a Frechet extreme value distribution, the sample mean will be dominated by a few large values. This results both in the large
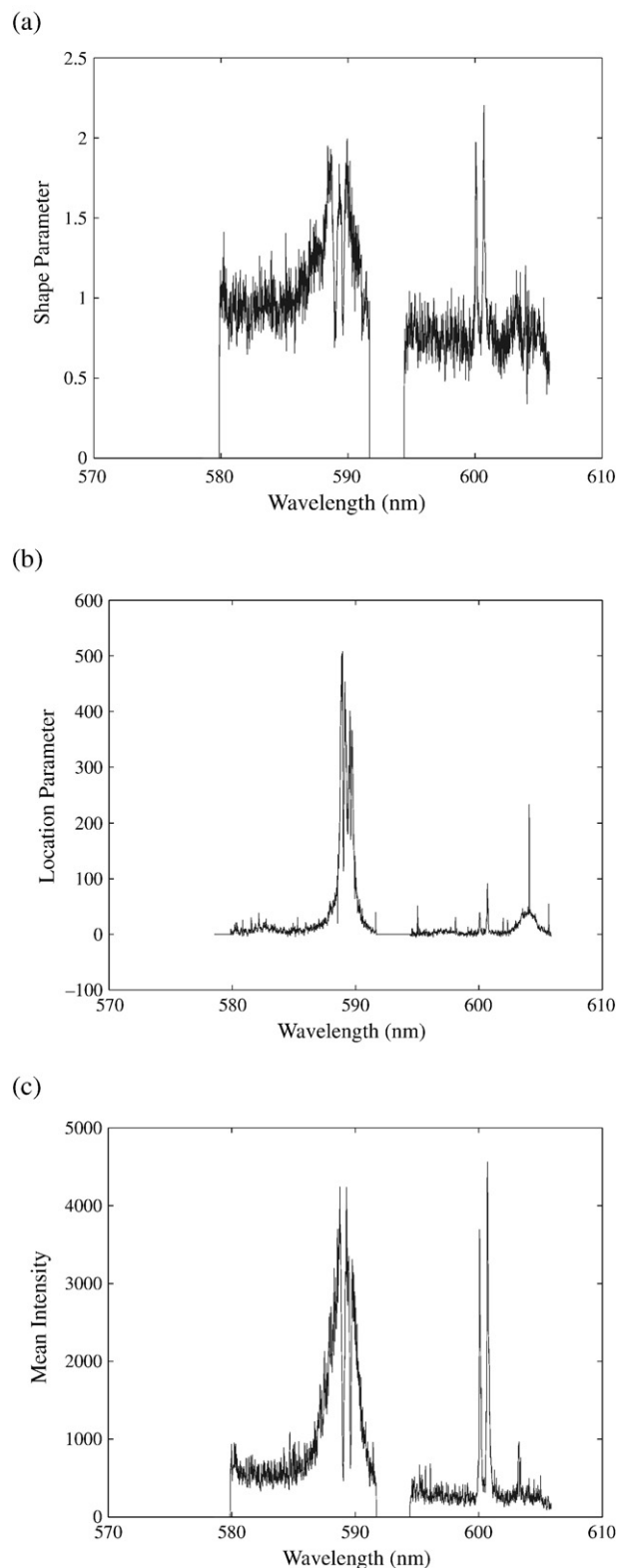
(a)

(b)

(c)

Fig. 6. (a) Shape parameter, (b) location parameter, and (c) sample mean for halite using the Echelle set-up.

wavelength-to-wavelength variability that is apparent in the sample mean and the substantial difference in amplitude between the sample mean and the location parameter. In addition, two large peaks are observed above 600 nm that are barely visible in the
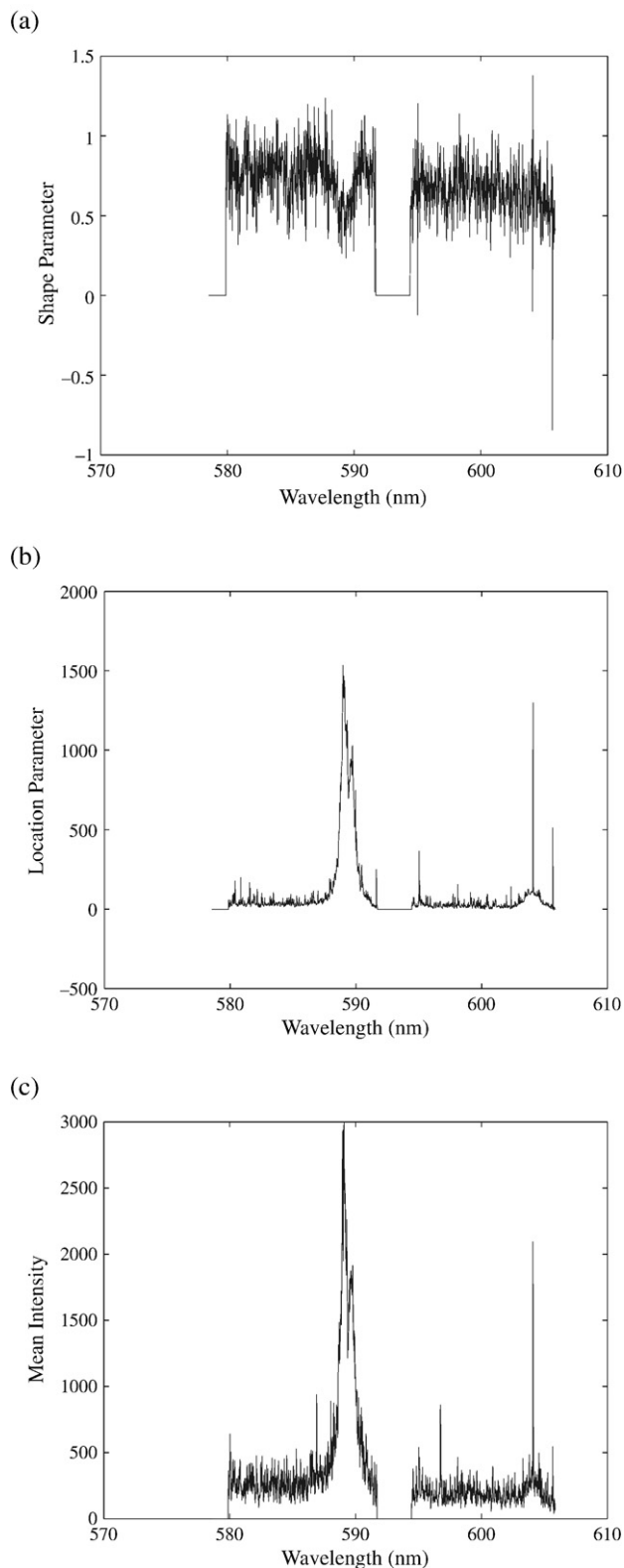
(a)

(b)

(c)

Fig. 7. (a) Shape parameter, (b) location parameter, and (c) sample mean for bulk aqueous solution using the Echelle set-up.
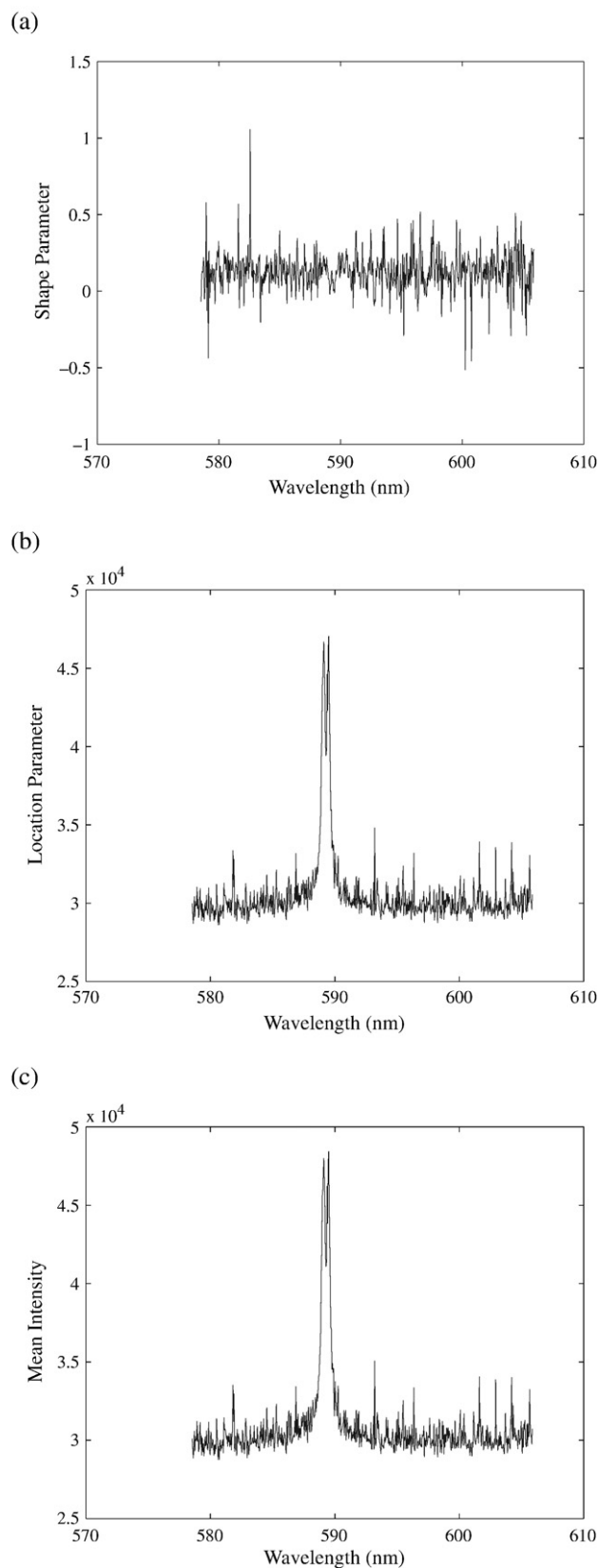
(a)

(b)

(c)

Fig. 8. (a) Shape parameter, (b) location parameter, and (c) sample mean for bulk aqueous solution using the Czerny–Turner set-up.

extreme value location parameter. These correspond to peaks well above 1.0 in the shape parameter where the extreme value distribution is very long-tailed, and serve as graphic illustration of the sort of erroneous conclusions that can be derived through use of inappropriate statistical estimators.

Fig. 7 compares the shape parameter, the location parameter, and the sample mean for Na in bulk aqueous solution using the Echelle set-up. The shape parameter is much more uniform with wavelength than for halite (Fig. 6), but persistently lies around 0.75 where the variance does not exist. As a consequence, the extreme value location parameter displays much less variability than the sample mean, as in Fig. 6. Fig. 7 is another example where the use of a standard sample mean estimator may lead to incorrect inferences.

Fig. 8 compares the shape parameter, the location parameter, and the sample mean for Na in bulk aqueous solution using the Czerny–Turner set-up. In contrast to the results with the Echelle set-up, the shape parameter is persistently below 0.5, and displays occasional excursions below 0 where the distribution is Weibull. Since both the mean and variance exist throughout the wavelength domain, the extreme value location parameter and the sample mean yield qualitatively similar results. However, the distribution remains extreme value rather than simple Gaussian, and the uncertainty inferred for the sample mean will be inaccurate.

While LIBS intensity data (whether single shot or analog accumulated) empirically appear to persistently be drawn from an extreme value distribution, systematic differences are observed between different experimental set-ups. Whether this is due to the spectrometer or laser design, the experimental geometry, the element under study or some other factor remains unknown. Since incorrect conclusions might be drawn from the use of an inappropriate statistical model, it is strongly urged that
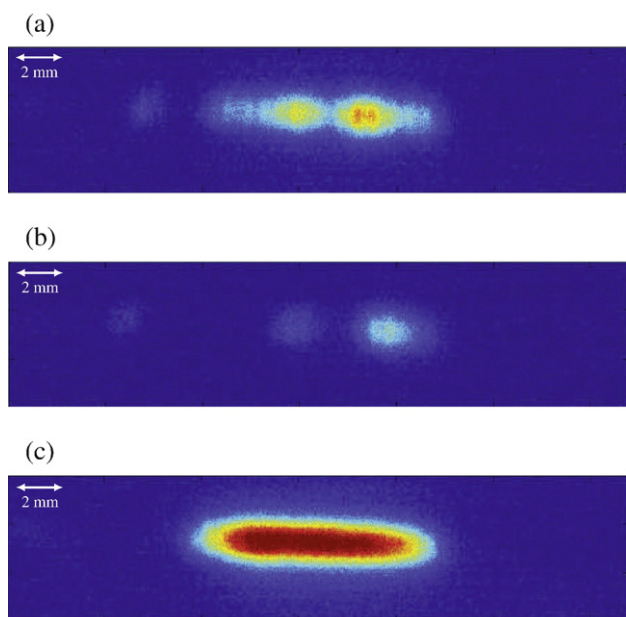

(a)

(b)

(c)

Fig. 9. Images of plasmas formed in bulk aqueous solution that illustrate the shot-to-shot variability of formation. Images were taken orthogonal to the incoming laser beam. In the images shown, the beam enters from the left. Plasmas were formed using 80 mJ of laser pulse energy.
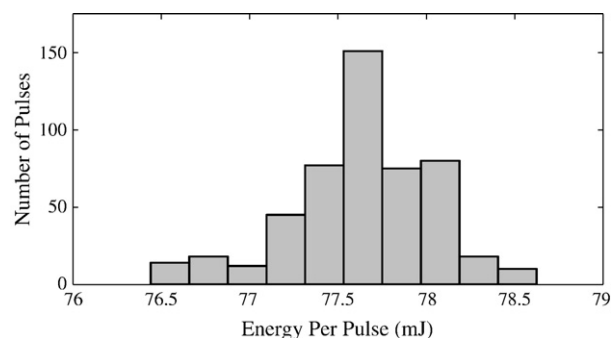

Fig. 10. Comparison of laser energies measured for 500 individual laser pulses.

LIBS practitioners examine their data to determine the correct approach for each set-up and sample.

3.4. Variability

In an attempt to understand the source of data variability, images of plasmas in liquids were taken and the energies of numerous single shot laser pulses were compared. Fig. 9 shows three sample plasma images taken under the same conditions that visually demonstrate the significant variability of plasma formation. The images are time averaged over 5 µs. Although hundreds of plasma images were taken, these images were selected to illustrate the variation in intensity, size, and location of formation of the plasma within a bulk liquid. The plasma shown in Fig. 9(c) displays significantly greater emission intensity and size than those in (a) and (b), illustrating the extreme nature of some plasmas. In contrast, the plasma in Fig. 9(b) is very weak, with very little emission produced. The distinct differences shown between these three plasmas is a clear indication that on a shot-to-shot basis that plasma variability exists and that extreme plasmas are formed which could account for the extreme intensities recorded.

The energy of 500 laser pulses was measured to examine the contribution of laser pulse energy fluctuations to plasma variability. Fig. 10 shows that shot-to-shot pulse energy fluctuations do exist; however, the variability is not extreme in nature, suggesting that laser pulse energy variation is not the dominant cause of plasma and peak intensity variations. This suggests that the variability of the plasma formation is due to other effects.

4. Conclusions

Examination of the variability of peak intensity for both single shot and analog accumulated LIBS spectra reveals that such data are drawn from an extreme value distribution. In many instances, the distribution has no variance, and in some cases the mean is also undefined. Under either circumstance, the use of the sample mean or variants that include censoring will be statistically inconsistent and the central limit theorem will not apply. A maximum likelihood estimator data processing scheme is presented that accurately deals with the extreme value nature of laser-induced plasma formation. It is strongly urged that this approach be used to ensure accurate scientific inference from LIBS data, and that use of estimators based on the sample mean be discontinued. Plasma images reveal large spatial and

intensity differences on a shot-to-shot basis. Laser pulse energy fluctuations are shown to contribute to the variability but are not the primary source.

References

[1] E. Tognoni, V. Palleschi, M. Corsi, G. Cristoforetti, N. Omenetto, I. Gornushkin, B.W. Smith, J.D. Winefordner, Laser-Induced Breakdown Spectroscopy (LIBS): fundamentals and applications, From Sample to Signal in LIBS, Cambridge University Press, 2006, pp. 122–170.

[2] V. Lazic, F. Colao, R. Fantoni, V. Spizzicchino, Laser-induced breakdown spectroscopy in water: improvement of the detection threshold by signal processing, Spectrochim. Acta Part B 60 (2005) 1002–1013.

[3] D.A. Cremers, L.J. Radziemski, Handbook of Laser-Induced Breakdown Spectroscopy, John Wiley and Sons, Ltd., 2006.

[4] D.A. Rusak, B.C. Castle, B.W. Smith, J.D. Winefordner, Recent trends and the future of laser-induced plasma spectroscopy, Trends Anal. Chem. 17 (1998) 453–461.

[5] V. Hohreiter, J.E. Carranza, D.W. Hahn, Temporal analysis of laser-induced plasma properties as related to laser-induced breakdown spectroscopy, Spectrochim. Acta Part B 59 (2004) 327–333.

[6] C.V. Bindhu, S.S. Harilal, M.S. Tillack, F. Najmabadi, A.C. Gaeris, Energy absorption and propagation in laser-created sparks, Appl. Spectrosc. 58 (6) (2004) 719–726.

[7] R. Wisbrun, I. Schechter, R. Niessner, H. Schroder, K.L. Kompa, Detector for trace elemental analysis of solid environmental samples by laser plasma spectroscopy, Anal. Chem. 66 (1994) 2964–2975.

[8] L. Xu, V. Bulatov, V.V. Gridin, I. Schechter, Absolute analysis of particulate materials by laser-induced breakdown spectroscopy, Anal. Chem. 69 (1997) 2103–2108.

[9] C.V. Bindhu, S.S. Harilal, M.S. Tillack, F. Najmabadi, A.C. Gaeris, Laser propagation and energy absorption by an argon spark, J. Appl. Phys. 94 (2003) 7402–7407.

[10] V. Lazic, F. Colao, R. Fantoni, V. Spizzicchino, Recognition of archeological materials underwater by laser induced breakdown spectroscopy, Spectrochim. Acta Part B 60 (2005) 1014–1024.

[11] J. Huang, C. Ke, K. Lin, Matrix effect on emission/current correlated analysis in laser-induced breakdown spectroscopy of liquid droplets, Spectrochim. Acta Part B 59 (2004) 321–326.

[12] U. Panne, C. Haisch, M. Clara, R. Niessner, Analysis of glass and glass melts during the vitrification process of fly and bottom ashes by laser-induced plasma spectroscopy. Part I: Normalization and plasma diagnostics, Spectrochim. Acta Part B 53 (1998) 1957–1968.

[13] B.C. Castle, K. Talabardon, B.W. Smith, J.D. Winefordner, Variables influencing the precision of laser-induced breakdown spectroscopy measurements, Appl. Spectrosc. 52 (1998) 649–657.

[14] G.A. Lithgow, S.G. Buckley, Effects of focal volume and spatial inhomogeneity on uncertainty in single-aerosol laser-induced breakdown spectroscopy measurements, Appl. Phys. Lett. 87 (2005) (011501–1–011501–3).

[15] I. Schechter, Direct aerosol analysis by time resolved laser plasma spectroscopy-improvement by single shot measurements, Analysis Sci. Technol. 8 (1995) 779–786.

[16] J.E. Carranza, D.W. Hahn, Sampling statistics and considerations for single-shot analysis using laser-induced breakdown spectroscopy, Spectrochim. Acta Part B 57 (2002) 779–790.

[17] P.K. Kennedy, D.X. Hammer, B.A. Rockwell, Laser-induced breakdown in aqueous media, Prog. Quant. Electron. 21 (1997) 155–248.

[18] Y. Ito, O. Ueki, S. Nakamura, Determination of colloidal iron in water by laser-induced breakdown spectroscopy, Anal. Chim. Acta 299 (1995) 401–405.

[19] N.F. Bunkin, A.V. Lobeyev, Influence of dissolved gas on optical breakdown and small-angle scattering of light in liquids, Phys. Lett., A 229 (1997) 327–333.

[20] U. Panne, D. Hahn, Laser-Induced Breakdown Spectroscopy (LIBS) fundamentals and applications, Analysis of Aerosols by LIBS, Cambridge University Press, 2006, pp. 194–253.

[21] S. Kotz, S. Nadarajah, Extreme Value Distributions: Theory and Applications, Imperial College Press, 2000.

[22] N.L. Johnson, S. Kotz, N. Balakrishnan, 2nd ed., Continuous Univariate Distributions, vol. 2, John Wiley & Sons, 1995.

[23] E.L. Lehmann, J.P. Romano, Testing Statistical Hypotheses, 3rd ed. Springer, 2005 (section 14.2).